NASA Contractor Report 185307

Optimization of Interface Layers in the Design of Ceramic Fiber Reinforced Metal Matrix Composites

I. Doghri, S. Jansson, F.A. Leckie, and J. Lemaitre
University of California
Santa Barbara, California

November 1990

Prepared for
Lewis Research Center
Under Grant NAG3-894

National Aeronautics and
Space Administration

OPTIMIZATION OF INTERFACE LAYERS IN THE DESIGN OF CERAMIC FIBER REINFORCED METAL MATRIX COMPOSITES

I. Doghri, S. Jansson, F.A. Leckie and J. Lemaitre*

Department of Mechanical and Environmental Engineering

University of California

Santa Barbara, CA 93106

ABSTRACT

The potential of using interface layer to reduce thermal stresses in the matrix of composites with a mismatch in coefficients of thermal expansion (CTE) of fiber and matrix has been investigated. It was found that the performance of the layer can be defined by the product of the CTE and the thickness, and that a compensating layer with a sufficiently high CTE can reduce the thermal stresses in the matrix significantly. A practical procedure offering a window of candidate layer materials is proposed.

---

*Visiting Professor from Université Paris 6, LMT Cachan, 61 Avenue du Président Wilson, 94230 Cachan, France

INTRODUCTION

Metal matrix composites reinforced with ceramic fibers are attractive because of their high specific stiffness and strength. Advantage can be taken from the high temperature strength of ceramic fibers and the ductility of the metal matrix to produce a composite with superior combined properties. However, a thermal mismatch exists between the ceramics fibers and the metal matrix: the ceramics having a low coefficient of thermal expansion (CTE) and metals have higher values of CTE. This thermal mismatch induces stresses in the composite when subjected to temperature change. Matrix cracking has been observed after cooling down from processing temperature to room temperature for brittle matrix materials [1]. It has been proposed that the addition of an interface layer between the fiber and the matrix can reduce the tensile residual stresses in the matrix to a level which is low enough to avoid matrix cracking.

Some numerical parametric studies have been performed [2], [3] in an attempt to determine the material parameters which are most beneficial in reducing thermal stresses. It has been suggested that the optimum interface layer should have a CTE between those of the matrix and fiber, with a low allowable modulus and a high layer thickness. A subsequent simplified analysis which retains the dominant physical features of the problem [4] showed that a compliant layer could not reduce the stresses in the matrix significantly. However, a layer with a high CTE, compensating layer, can reduce the stresses in the matrix significantly. The purpose of this study is to detremine the validity of the simplified method and to produce results which are useful for design.

The study is based on a 3 cylinder model, isolating one fiber with an interface layer and a matrix layer (Fig. 1). Only monotonic cooling is studied and the variation of the materials properties with temperature is not considered. In a first part, the results of the simplified analysis which assumes a rigid fiber and a very thin layer, are recapitulated. This analysis identifies the properties of an interface layer. In the second part, the assumptions made previously are released and a complete elastic analysis is performed assuming that the three materials are isotropic and linearly elastic. A systematic parametric

study is also conducted and a practical procedure offering a window of candidate layer materials is proposed.

In a later study [5] both the interface layer and the matrix are considered to be elastic-plastic, and the temperature dependence of the properties of the 3 materials is considered. In addition to the 3 cylinder model, a unit cell of a hexagonal array of the fibrous composite is defined and finite element computations are performed under several thermal-mechanical loadings.

NOTATIONS

f	fiber
ℓ	interface layer
m	matrix
j	f, ℓ, m
R_j	external radius of j
$t_\ell = R_\ell - R_f$	layer thickness
E_j	Young's modulus of j
ν_j	Poisson's ratio of j
λ_j and μ_j	Lamé coefficients of j

$$\lambda_j = \frac{E_j \nu_j}{(1-2\nu_j)(1+\nu_j)} \quad , \quad \mu_j = \frac{E_j}{2(1+\nu_j)}$$

α_j	CTE of j
ΔT	change in temperature
σ_{rj}	radial stress (σ_{rr}) in j
$\sigma_{\theta j}$	hoop stress ($\sigma_{\theta\theta}$) in j
σ_{zj}	longitudinal stress (σ_{zz}) in j
ε_{rj}	radial strain (ε_{rr}) in j
$\varepsilon_{\theta j}$	hoop strain ($\varepsilon_{\theta\theta}$) in j
ε_{zj}	longitudinal strain (ε_{zz}) in j
$\overline{\sigma}_j$	Mises equivalent stress in j

The radii R_f and R_m are related to the fiber volume fraction C_f by the relation

$$C_f = \left(\frac{R_f}{R_m}\right)^2$$

1. SIMPLIFIED ELASTIC ANALYSIS

1.1 *Stress-Strain Analysis*

Ceramics fibers are usually four to five times stiffer than the metal matrix materials. Hence, in order to simplify the calculations, it is assumed that

$$\frac{E_f}{E_m} >> 1 \qquad \text{and} \qquad \frac{E_f}{E_\ell} >> 1$$

The fiber volume fraction, C_f is assumed to be of the same order as the matrix volume fraction so that

$$\frac{C_f}{1-C_f} \cong 1$$

For the given assumptions the stiff fiber controls the thermal expansion in the axial direction of the cylinder model. Hence, the stress distribution in the matrix and interface layer is governed by a plane strain problem with a fixed inner radius at the fiber interface. The analysis reveals that the differential CTE's of matrix and fiber, and interface layer and fiber dictate the thermal stresses. Consequently, the differential CTEs are defined as

$$\Delta\alpha_m = \alpha_m - \alpha_f \quad \text{and} \quad \Delta\alpha_\ell = \alpha_\ell - \alpha_f$$

The stress distribution in the matrix is given by the plane strain solution for a thick walled cylinder subjected to an unknown internal pressure p, a traction free outer surface, and a temperature change ΔT. Superimposing the solutions given in [6] for an internal pressure and a temperature change gives the stress distributions in the matrix

$$\sigma_{rm} = -p\frac{(R_m/r)^2 - 1}{(R_m/R_f)^2 - 1}$$

$$\sigma_{\theta m} = p\frac{(R_m / r)^2 + 1}{(R_m / R_f)^2 - 1}$$

$$\sigma_{zm} = p\frac{2\nu_m}{(R_m / R_f)^2 - 1} + E_m\,\Delta\alpha_m\,\Delta T$$

The highest stresses in the matrix occur at the inner surface of the cylinder, $r = R_f$. The von Mises equivalent stress

$$\overline{\sigma} = \sqrt{\sigma_r^2 + \sigma_\theta^2 + \sigma_z^2 - \sigma_r\sigma_\theta - \sigma_r\sigma_z - \sigma_\theta\sigma_z}$$

can be calculated as

$$\overline{\sigma}_m = \left\{\left[p\frac{C_f}{1-C_f}\right]^2 [3/C_f^2 + 1 - 4\nu_m(1-\nu_m)] - pE_m\Delta\alpha_m\Delta T\frac{C_f}{1-C_f}2[1-2\nu_m]\right.$$

$$\left. + [E_m\Delta\alpha_m\Delta T]^2\right\}^{1/2}$$

The layer is subjected to a pressure in the radial direction resulting from the contact with the matrix

$$\sigma_{r\ell} = -p$$

The temperature change ΔT introduces stresses in the hoop and longitudinal directions due to the constraint from the fibers. The stresses in the hoop and longitudinal directions are equal and are the sum of the stresses caused by the pressure and the thermal expansion

$$\sigma_{\theta\ell} = \sigma_{z\ell} = -\frac{\nu_\ell}{1-\nu_\ell}p + \frac{1}{1-\nu_\ell}E_\ell\Delta\alpha_\ell\Delta T$$

The von Mises equivalent stress in the layer is given by

$$\bar{\sigma}_\ell = \frac{1}{1-\nu_\ell}\left|E_\ell \Delta\alpha_\ell \Delta T + (1-2\nu_\ell)p\right|$$

Compatibility in the radial displacement at the boundary between the inner surface of the matrix and the interface layer is the condition which isolates the value of p which is found to be

$$p = \frac{[1+\nu_m] - \dfrac{t_\ell \Delta\alpha_\ell}{R_f \Delta\alpha_m}\dfrac{1+\nu_\ell}{1-\nu_\ell}}{\left(1-\nu_m^2\right)\left[\dfrac{1+C_f}{1-C_f} + \dfrac{\nu_m}{1-\nu_m}\right] + \dfrac{t_\ell E_m}{R_f E_\ell}\dfrac{\nu_\ell}{1-\nu_\ell}} E_m \Delta\alpha_m \Delta T$$

1.2 *Sensitivity Study*

1.2.1 Stresses in the matrix

The term $E_m \Delta\alpha_m \Delta T$ enters in all the expressions for stress and all results are normalized with respect to this term. The stresses at the inner radius of the matrix are shown in Fig. 2 as a function of normalized pressure for a fiber volume fraction $C_f = 0.4$ in a Ti_3Al matrix with $\nu_m = 0.25$. It can be seen that a pressure at the interface causes increased tensile stresses in the hoop and axial direction that could cause matrix cracking, initiated from defects at the fiber matrix interface.

The value of the critical stress for matrix cracking, σ_{cm}, sets an upper limit for the principal stresses $\sigma_{\theta m}$, σ_{zm}, and σ_{rm} and defines bounds on the pressure p if matrix failure is to be avoided. The allowable equivalent stress, σ_{ym}, in the matrix defines other bounds on the pressure. These conditions define a window for the interface pressure, Fig. 2, so that the failure criteria are not violated.

Inspection of the expression of p reveals that the pressure may be reduced by the introduction of a compliant layer with low modulus which would increase the denominator, but the second term in the denominator of p is usually sufficiently small to be neglected in

the calculations and the pressure is then linearly dependent on the parameter $\frac{\Delta\alpha_\ell t_\ell}{\Delta\alpha_m R_f}$. This effect is demonstrated in Fig. 3 where it can be seen that the influence of $\frac{E_m t_\ell}{E_\ell R_f}$ is small. Figure 2 shows that the Mises equivalent stress has a minimum for an interface pressure that is close to zero. The pressure p is zero when

$$\frac{\Delta\alpha_\ell t_\ell}{\Delta\alpha_m R_f} = (1+\nu_m)\frac{(1-\nu_\ell)}{1+\nu_\ell}$$

from which it can be deduced that the stresses in the matrix are strongly influenced by the parameter $\Delta\alpha_\ell t_\ell$. The results from Fig. 2 and Fig. 3 can then be combined in Fig. 4 where the highest principal stress and equivalent stress at the inner radius of the matrix cylinder are plotted versus the parameter $\Delta\alpha_\ell t_\ell/\Delta\alpha_m R_f$.

If the pressure is to be reduced to a minimum, the differential CTE for the layer has to be $\Delta\alpha_\ell \simeq 6\Delta\alpha_m$, when $t_\ell/R_f = 0.1$ For the case of SiC fibers, $\alpha_f \simeq 5 \times 10^{-6}/°C$ in a Ti_3Al matrix, $\alpha_m \simeq 10 \times 10^{-6}$, requires that $\alpha_\ell \simeq 35 \times 10^{-6}$. Handbook values [7] of metals with a reasonably high melting point and high CTE are: silver 26×10^{-6}, hafnium 500×10^{-6} and copper 17×10^{-6}. It is evident therefore that an interface layer of readily available materials with high CTE has the potential of substantially reducing thermal stresses in the matrix.

1.2.2 Stresses in the Interface Layer

The tradeoff for the improved stress state in the matrix is that the thermal mismatch has to be taken up by the interface layer. The deformation of the layer is constrained in the hoop and longitudinal direction so that tensile stresses develop in the layer. The highest principal stress in the interface layer is shown in Fig. 5 as a function of the different dimensionless parameters defining the problem. The stress is strongly dependent on the layer modulus, E_ℓ/E_m, and CTE, $\Delta\alpha_\ell/\Delta\alpha_m$, but weakly dependent on the layer thickness t_ℓ/R_f. This indicates that the stress is dominated by the constrained thermal expansion,

which is given by the second term in the stress expression, and is weakly dependent on the interface pressure, the first term in this expression. The product $\Delta\alpha_\ell t_\ell$ governs the reduction of stress in the matrix, Fig. 4, and has to have a required value to reducing the stresses in the matrix to an acceptable level. It can be deducted from Fig. 4 and Fig. 5 that it is more favorable to have a thick layer and a moderate high layer CTE than a thin layer and a high layer CTE in order to fulfill the requirement of stress reduction in the matrix and to avoid high tensile stresses in the layer.

2. ELASTIC ANALYSIS

2.1 *Stress-strain Analysis*

The composite is not subjected to transverse loading and the outer surface of the compound cylinder is traction free. The thermal loading is axisymmetric with respect to the z-axis, then the displacement in the transverse plane is radial: $U_j(r)$. The fibers are long and the stress and strain distributions are constant in the z-direction except at the end regions which will not be studied here. A generalized plane strain assumption is made: ε_{zj} = constant = e_z. The other strains are given by:

$$\varepsilon_{rj} = U_j' \quad \text{and} \quad \varepsilon_{\theta j} = \frac{U_j}{r}$$

and there are no shear strains.

The linear thermo-elastic behavior gives the stresses as

$$\sigma_{rj} = \lambda_j\left(U_j' + \frac{U_j}{r} + e_z\right) + 2\mu_j U_j' - \left(3\lambda_j + 2\mu_j\right)\alpha_j \Delta T$$

$$\sigma_{\theta j} = \lambda_j\left(U_j' + \frac{U_j}{r} + e_z\right) + 2\mu_j \frac{U_j}{r} - \left(3\lambda_j + 2\mu_j\right)\alpha_j \Delta T$$

$$\sigma_{zj} = \lambda_j\left(U_j' + \frac{U_j}{r} + e_z\right) + 2\mu_j e_z - \left(3\lambda_j + 2\mu_j\right)\alpha_j \Delta T$$

The equilibrium equations in cylindrical coordinates give:

$$\frac{\partial \sigma_{rj}}{\partial r} + \frac{1}{r}\left(\sigma_{rj} - \sigma_{\theta j}\right) = 0$$

which gives the displacement field as

$$U_j = c_j r + D_j \frac{R_j^2}{r}$$

where c_j and D_j are constants to be found by the boundary conditions. We have $D_f = 0$ in order to obtain a finite solution in (f).

To summarize, the strains are given by

$$\varepsilon_{rj} = c_j - \left(\frac{R_j}{r}\right)^2 D_j$$

$$\varepsilon_{\theta j} = c_j + \left(\frac{R_j}{r}\right)^2 D_j$$

$$\varepsilon_{zj} = e_z = \text{ constant}$$

The stresses are defined by

$$\sigma_{rj} = 2(\lambda_j + \mu_j)c_j + \lambda_j e_z - 2\mu_j \left(\frac{R_j}{r}\right)^2 D_j - (3\lambda_j + 2\mu_j)\alpha_j \Delta T$$

$$\sigma_{\theta j} = 2(\lambda_j + \mu_j)c_j + \lambda_j e_z + 2\mu_j \left(\frac{R_j}{r}\right)^2 D_j - (3\lambda_j + 2\mu_j)\alpha_j \Delta T$$

$$\sigma_{zj} = 2\lambda_j c_j + (\lambda_j + 2\mu_j)e_z - (3\lambda_j + 2\mu_j)\alpha_j \Delta T$$

The strains and the stresses are uniform in the fiber. The axial strain is constant in the whole composite and the axial stresses are uniform in (ℓ) and (m). The Mises equivalent stress $\overline{\sigma}_j$ is defined by

$$\overline{\sigma}_j^2 = \frac{1}{2}\left[\left(\sigma_{rj}-\sigma_{\theta j}\right)^2+\left(\sigma_{\theta j}-\sigma_{zj}\right)^2+\left(\sigma_{rj}-\sigma_{zj}\right)^2\right]$$

$$= 4\mu_j^2\left[3\left(\frac{R_j}{r}\right)^4 D_j^2+\left(c_j-e_z\right)^2\right]$$

The six unknown c_f, c_ℓ, D_ℓ, c_m, D_m and e_z are determined by the following conditions:

$$U_f = U_\ell \text{ at } r = R_f$$
$$U_\ell = U_m \text{ at } r = R_\ell$$
$$\sigma_{rf} = \sigma_{r\ell} \text{ at } r = R_f$$
$$\sigma_{r\ell} = \sigma_{rm} \text{ at } r = R_\ell$$
$$\sigma_{rm} = 0 \text{ at } r = R_m$$

$$2\pi\int_0^{R_m}\sigma_{zj}rdr = 0 \Rightarrow R_f^2\sigma_{zf}+\left(R_\ell^2-R_f^2\right)\sigma_{z\ell}+\left(R_m^2-R_\ell^2\right)\sigma_{zm} = 0$$

The linear system obtained is given in Appendix I.

Since $\sigma_{rm}(R_m) = 0$, the stresses in the matrix can also be written as

$$\sigma_{rm} = 2\mu_m D_m\left[1-\left(\frac{R_m}{r}\right)^2\right]$$

$$\sigma_{\theta m} = 2\mu_m D_m\left[1+\left(\frac{R_m}{r}\right)^2\right]$$

$$\sigma_{zm} = 2\mu_m[D_m - c_m + e_z]$$

It is reasonable to assume that $D_m \geq 0$ (because this gives a compressive σ_{rm} and a tensile $\sigma_{\theta m}$). In this case, it is obvious that the minimal hoop stress is obtained for $D_m = 0$, which gives $\sigma_{rm} = 0$ and $\sigma_{\theta m} = 0$, i.e. a uniaxial longitudinal stress state. This result was confirmed numerically (see Section 2.3).

2.2 Sensitivity Study

The properties of the interface layer are defined by the four parameters: E_ℓ, ν_ℓ, α_ℓ and t_ℓ. A sensitivity study was conducted in order to measure the influence of each of these parameters on the reduction of the residual stresses in the matrix. As a conclusion to this study, a procedure allowing the choice of candidate interface layer materials is proposed in Section 2.3.

The fiber and the matrix are defined by the following data

- Fiber: SiC (SCS6)
  $E_f = 360$ GPa, $\nu_f = 0.17$, $\alpha_f = 4.9 \times 10^{-6}/°C$
- Matrix: Ti_3Al
  $E_m = 75.2$ GPa, $\nu_m = 0.25$, $\alpha_m = 11.7 \times 10^{-6}/°C$

The radii R_f and R_m are related to the fiber volume fraction by

$$C_f = \left(\frac{R_f}{R_m}\right)^2 \cong 40.5\%$$

The characteristics of the fiber and the matrix were kept constant but the parametric study can be readily applied to fibers and matrix with other properties.

The range of interface layer parameters were chosen as follows:

$$69 \leq E_\ell \leq 517 \quad \text{GPa}$$

$$4 \leq \alpha_\ell \leq 30 \quad \text{x } 10^{-6}/°C$$

$$0.028 \leq \frac{t_\ell}{R_f} \leq 0.28$$

The Poisson's ratio of the layer ν_ℓ was kept constant: $\nu_\ell = 0.3$.

To study the impact of the interface layer, a reference state was defined which corresponds to the state of stresses in the matrix in a 2 cyclinder without the layer. The stresses in the 3 cylinder model have been normalized with the reference stresses. The stresses in the layer and matrix are given at the inner radii.

2.2.1 Influence of the Young's Modulus E_ℓ (α_ℓ, t_ℓ fixed)

The results of the sensitivity study have shown that in the range 69 + 200 GPA, the value of E_ℓ has little influence on matrix stresses (Fig. 6a). If $E_\ell = 200 + 517$ GPA, then

- if $\alpha_\ell \leq 10 \text{ x } 10^{-6}/°C$, the value of $\bar{\sigma}_m$ is again independent of the value of E_ℓ (Fig. 6a).
- if $\alpha_\ell > 10 \text{ x } 10^{-6}/°C$, the increase of E_ℓ may reduce the stresses in (m) but increase the stresses in (ℓ) to unacceptable values (see Fig. 6a and 6b).

For the remaining of this study, we will choose $E_\ell \leq 200$ GPa. This is not too restrictive because an important property of the interface layer is a high value of CTE (see discussion in section 1.2) so that the layer is likely to be a metal for which the Young modulus is usually lower than 200 GPa.

2.2.2 Influence of the CTE α_ℓ (E_ℓ, t_ℓ fixed)

The results show that generally the matrix equivalent stress $\bar{\sigma}_m$ decreases considerably as α_ℓ increases. However as illustrated in Fig. 7, the stresses reach a minimum after which they increase again with increasing α_ℓ.

The decrease of $\bar{\sigma}_m$ is more pronounced if the fixed thickness t_ℓ is high as is evident

from Fig. 7.

In all the cases $\frac{\bar{\sigma}_m}{\sigma_{ref}} \leq 1$: the addition of the interface layer does reduce the residual stresses in the matrix.

2.2.3 Influence of the Thickness t_ℓ (E_ℓ, α_ℓ fixed)

The results are qualitatively the same as for α_ℓ; i.e. in general $\bar{\sigma}_m$ decreases as t_ℓ increases (see Fig. 8).

2.2.4 A Convenient Parametric Representation

The conclusions of the above sensitivity analysis are in agreement with those of the simplified analysis [4] described in section 1. That analysis lead naturally to the graphical representation given in Fig. 4. In the analysis it was shown that the important layer parameter which affected the matrix stress is $\Delta\alpha_\ell t_\ell$. This graphical representation is used to present the results of the sensitivity study and they are given in Fig. 9. These results were generated using $E_\ell = E_m = 75.2$ GPa, and they are nearly the same for all values of E_ℓ lower than 200 GPa. The representation proves to be very useful since all the factors influencing the matrix stresses can be presented in one graph. Also shown in Fig. 9 are the results of the simplified analysis. The complete analysis predicts lower stresses than those from the simplified analysis, which is not surprising since the full analysis avoids assumptions which imply constraint.

The range of $x_\ell = \frac{\Delta\alpha_\ell t_\ell}{\Delta\alpha_m R_f}$ was limited to the domain of allowable pressure (defined in Fig. 2 and 3). The minimum value of $\bar{\sigma}_m$ corresponds to $x_\ell \simeq 0.65$. If $x_\ell > 0.65$, it was found that the radial stress in (m) becomes tensile and the hoop stress compressive ($\sigma_{rm} > 0$, $\sigma_{\theta m} < 0$, $\sigma_{zm} > 0$). Layers such that $x_\ell > 0.65$ are over-compensating layers.

2.3 *A Convenient Procedure to Choose Candidate Layer Materials*

The interface layer is defined by 4 parameters: E_ℓ, ν_ℓ, α_ℓ and t_ℓ. In the sensitivity study we kept the Poisson's ratio of the layer constant: $\nu_\ell = 0.3$ and we found that it is

reasonable to take the Young modulus of the layer in this range: $E_\ell = 69 \div 200$ GPa. So we kept $E_\ell = 69$ GPa = constant.

The matrix stresses can be readily calculated using Fig. 9. However, using this form requires further effort when making selection of the interface layer. This procedure is developed to deal with this situation. The axes used in the proposed graphs are the thickness of the layer and the CTE of the layer. The ratio of the matrix Mises equivalent stress with and without the layer is determined, and the graph shown in Fig. 10 then presents contours of constant reduction factor. Similarly in Figs. 11, 12, 13 the reduction factors for the damage stress, tensile hoop stress and tensile axial stress are plotted in an identical manner.

Reduction of the Mises equivalent stress:

It has been noticed that $\frac{\overline{\sigma}_f}{\overline{\sigma}_{ref}}$ and $\frac{\overline{\sigma}_\ell}{\overline{\sigma}_{ref}}$ decrease if α_ℓ decreases. So, for a given stress reduction inthe matrix (i.e. a given contour in Fig. 10) one can choose α_ℓ such that $\frac{\overline{\sigma}_\ell}{\overline{\sigma}_{ref}}$ does not exceed a certain value to avoid layer cracking. The min. value of $\frac{\overline{\sigma}_m}{\overline{\sigma}_{ref}}$ was found to be $\simeq 0.387$ (see shaded line in Fig. 10). This contour was also found to correspond to a uniaxial longitudinal stress state in the matrix (see remark at the end of section 2.1).

Reduction of the Damage Equivalent Stress

In the same way that the Mises equivalent stress is related to the distorsion energy, a so-called damage equivalent stress [8] is related to the total elastic energy and is defined by

$$\sigma^* = \overline{\sigma}\left[\frac{2}{3}(1+\nu) + 3(1-2\nu)\left(\frac{\sigma_H}{\overline{\sigma}}\right)^2\right]^{1/2}$$

where $\sigma_H = \frac{1}{3}\sigma_{kk}$.

One notices the presence of the triaxiality ratio $\frac{\sigma_H}{\overline{\sigma}}$ which is known to be a main feature in failure.

The contours of Fig. 11 can be used in the same way as those of the Mises stress. The same remark about the decrease of σ_f^* and σ_ℓ^* when α_ℓ decreases applies also. If we compare the contours of the Mises and the damage equivalent stresses, we find that:

i) In the "upper" region of the plane defined by $\alpha_\ell = 30\times10^{-6}/°C$, $\frac{t_\ell}{R_f} = 0.28$ and $\frac{\sigma_m^*}{\sigma_{ref}^*} = 0.387$ (shaded line) the criterion based on the reduction of the Mises stress is a bit more severe than the second one, i.e. for a given point $\left(\frac{t_\ell}{R_f}, \alpha_\ell\right)$ we have $\frac{\sigma^*}{\sigma_{ref}^*} \le \frac{\overline{\sigma}}{\overline{\sigma}_{ref}}$.

ii) In the remainder region, the criterion based on the reduction of the damage equivalent stress is a bit more severe than the first one. The reason is the following.

The calculations have shown that $\sigma_{ref}^* \cong \overline{\sigma}_{ref}$, so

$$\frac{\sigma^*}{\sigma_{ref}^*} \le \frac{\overline{\sigma}}{\overline{\sigma}_{ref}} \Rightarrow \left|\frac{\sigma_H}{\overline{\sigma}}\right| \le \frac{1}{3}$$

so, the triaxiality ratio in the matrix is

$\le \frac{1}{3}$ in the "upper" region i)

$\ge \frac{1}{3}$ in the remainder region ii)

Reduction of the Hoop Stress

It appears that the reduction of the hoop stress in (m) is much more important than the reduction of the Mises stress. The hoop stress can actually be decreased to a zero value, which is shown by the shaded line in Fig. 12. This line corresponds also to the min. Mises

stress and to a uniaxial z-stress in the matrix. In the "upper" region defined by the shaded line as previously, the hoop stress in (m) becomes compressive: $\sigma_{\theta m} < 0$. This region corresponds also to $x_\ell > 0.65$, as defined in section 2.2.4.

Reduction of the Longitudinal Stress

It appears that the reduction of σ_{zm} is smaller than the reduction of $\overline{\sigma}_m$ or $\sigma_{\theta m}$. The shaded line ($\overline{\sigma}_m$ minimal and $\sigma_{\theta m} = 0$) gives $\frac{\sigma_{zm}}{\sigma_{zref}} \cong 0.6$. A lower reduction cannot be expected and if the reduction of σ_{zm} is a concern, then the window of candidate layer materials is reduced as shown by comparing Fig. 13 to the previous figures.

CONCLUSIONS

The thermal mismatch between the fiber and the matrix has to be taken up by the interface layer and can subject it to high stresses if the Young modulus of the layer is high. If this modulus is taken in a certain range, common to most metals, then the layer performance is defined by the product of the CTE and the thickness.

A compensating layer with a sufficiently high CTE has the potential of reducing the thermal stresses in the matrix significantly. Both the CTE and the thickness of the layer can be adjusted in order to keep the stresses in the layer under a certain level. The maximum hoop stress in the matrix can be reduced substantially but the axial stress in the matrix is less affected by a layer. This implies that compensating layers can be expected to be very successful in preventing cracking in composites where predominantly radial cracking is observed in the matrix, but that while axial stresses can also be reduced, this reduction is less dramatic.

Graphs have been produced which are simple to use. From Figs. 10 to 13, the reduction in stress for any value of layer CTE and thickness are readily determined. The absolute values of matrix stress can be easily determined by reference from another diagram (Fig. 9).

APPENDIX: Linear System for the Constants of the Elastic Solution

$$\begin{bmatrix} 1 & -1 & -\left(\frac{R_\ell}{R_f}\right)^2 & 0 & 0 & 0 \\ 0 & 1 & 1 & -1 & -\left(\frac{R_m}{R_\ell}\right)^2 & 0 \\ 2(\lambda_f+\mu_f) & 0 & 2\mu_\ell\left[\left(\frac{R_\ell}{R_f}\right)^2-1\right] & 0 & 2\mu_m\left[\left(\frac{R_m}{R_\ell}\right)^2-1\right] & \lambda_f \\ 0 & 2(\lambda_\ell+\mu_\ell) & -2\mu_\ell & 0 & 2\mu_m\left[\left(\frac{R_m}{R_\ell}\right)^2-1\right] & \lambda_\ell \\ 0 & 0 & 0 & 2(\lambda_m+\mu_m) & -2\mu_m & \lambda_m \\ 2\lambda_f\left(\frac{R_f}{R_\ell}\right)^2 & 2\lambda_\ell\left[1-\left(\frac{R_f}{R_\ell}\right)^2\right] & 0 & 2\lambda_m\left[\left(\frac{R_m}{R_\ell}\right)^2-1\right] & 0 & A_{66} \end{bmatrix} \begin{bmatrix} C_f \\ C_\ell \\ D_\ell \\ C_m \\ D_m \\ e_z \end{bmatrix} = \begin{bmatrix} 0 \\ 0 \\ (3\lambda_f+2\mu_f)\alpha_f\Delta T \\ (3\lambda_\ell+2\mu_\ell)\alpha_\ell\Delta T \\ (3\lambda_m+2\mu_m)\alpha_m\Delta T \\ b_6 \end{bmatrix}$$

where

$$A_{66} = (\lambda_f+2\mu_f)\left(\frac{R_f}{R_\ell}\right)^2 + (\lambda_\ell+2\mu_\ell)\left[1-\left(\frac{R_f}{R_\ell}\right)^2\right] + (\lambda_m+2\mu_m)\left[\left(\frac{R_m}{R_\ell}\right)^2-1\right]$$

$$b_6 = b_3\cdot\left(\frac{R_f}{R_\ell}\right)^2 + b_4\cdot\left[1-\left(\frac{R_f}{R_\ell}\right)^2\right] + b_5\cdot\left[\left(\frac{R_m}{R_\ell}\right)^2-1\right]$$

REFERENCES

[1] Brindley, P.K., Bartolotta, P.A. and MacKay, R.A., "Thermal and Mechanical Fatigue of SiC/Ti_3Al+Nb," 2nd HITEMP Review, NASA CP-10039, paper 52, 1989.

[2] Ghosn, L.J. and Bradley, A.L., "Optimum Interface Properties for Metal Matrix Composites," NASA TM-102295, 1989.

[3] Caruso, J.J., Chamis, C.C. and Brown, H.C., "Parametric Studies to Determine the Effects of Compliant Layers on Metal Matrix Composite Systems," NASA TM-102465, 1990.

[4] Jansson, S. and Leckie, F.A., "Reduction of Thermal Stresses in Continuous Fiber Reinforced Metal Matrix Composites with Interface Layers," submitted for publication, 1990.

[5] Doghri, I. and Leckie, F.A., "Elasto-plastic Analysis of Interface Layers for Fiber Reinforced Metal Matrix Composites," submitted for publication, 1990.

[6] Timoshenko, S.P. and Goodier, J.N., "Theory of Elasticity," McGraw-Hill, Auckland, 1970.

[7] Boyer, H.E. and Gall, T.L., "Metals Handbood, Desk Edition," ASM, Metals Park, 1985.

[8] Lemaitre, J. and Chaboche, J.L., "Mechanics of Solid Materials," Cambridge University Press, 1990.

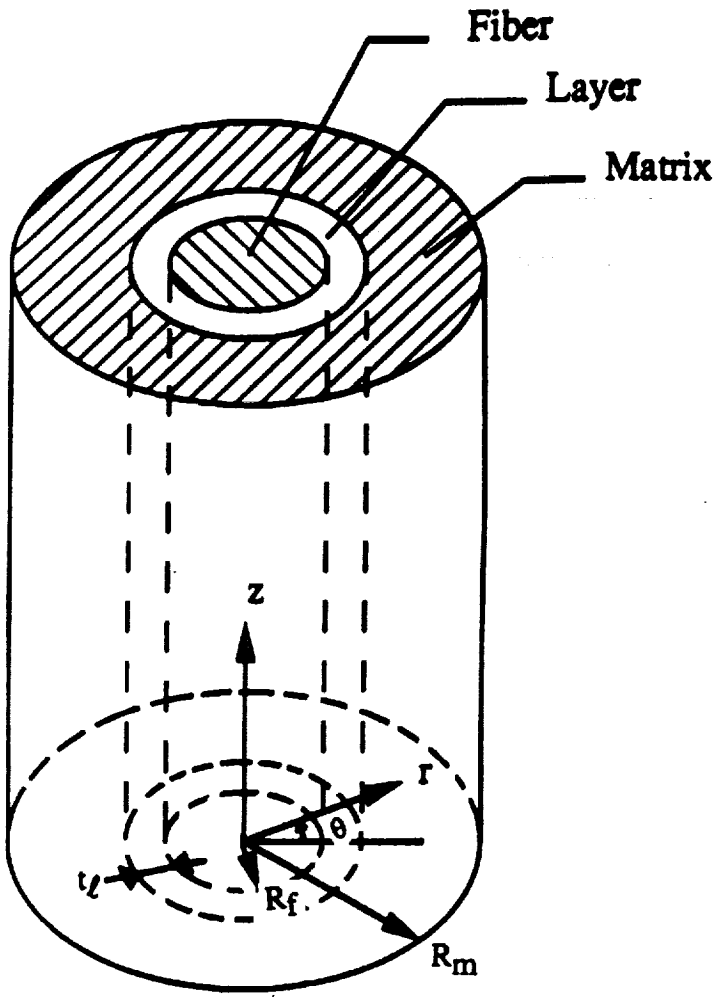

Fig. 1 Concentric 3 cylinder model.

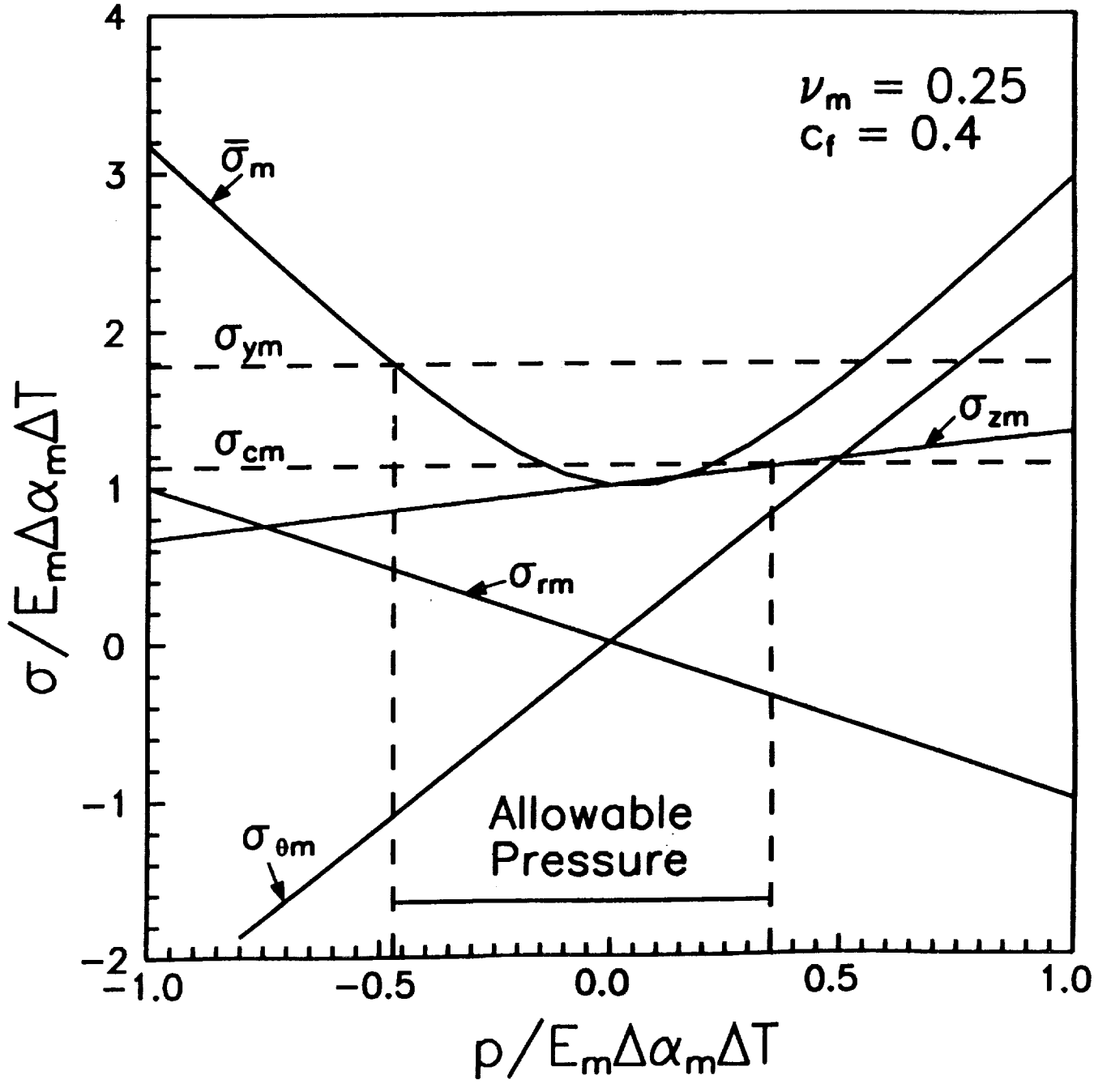

Fig. 2 Stresses at the inner surface of the matrix cylinder as a function of normalized pressure.

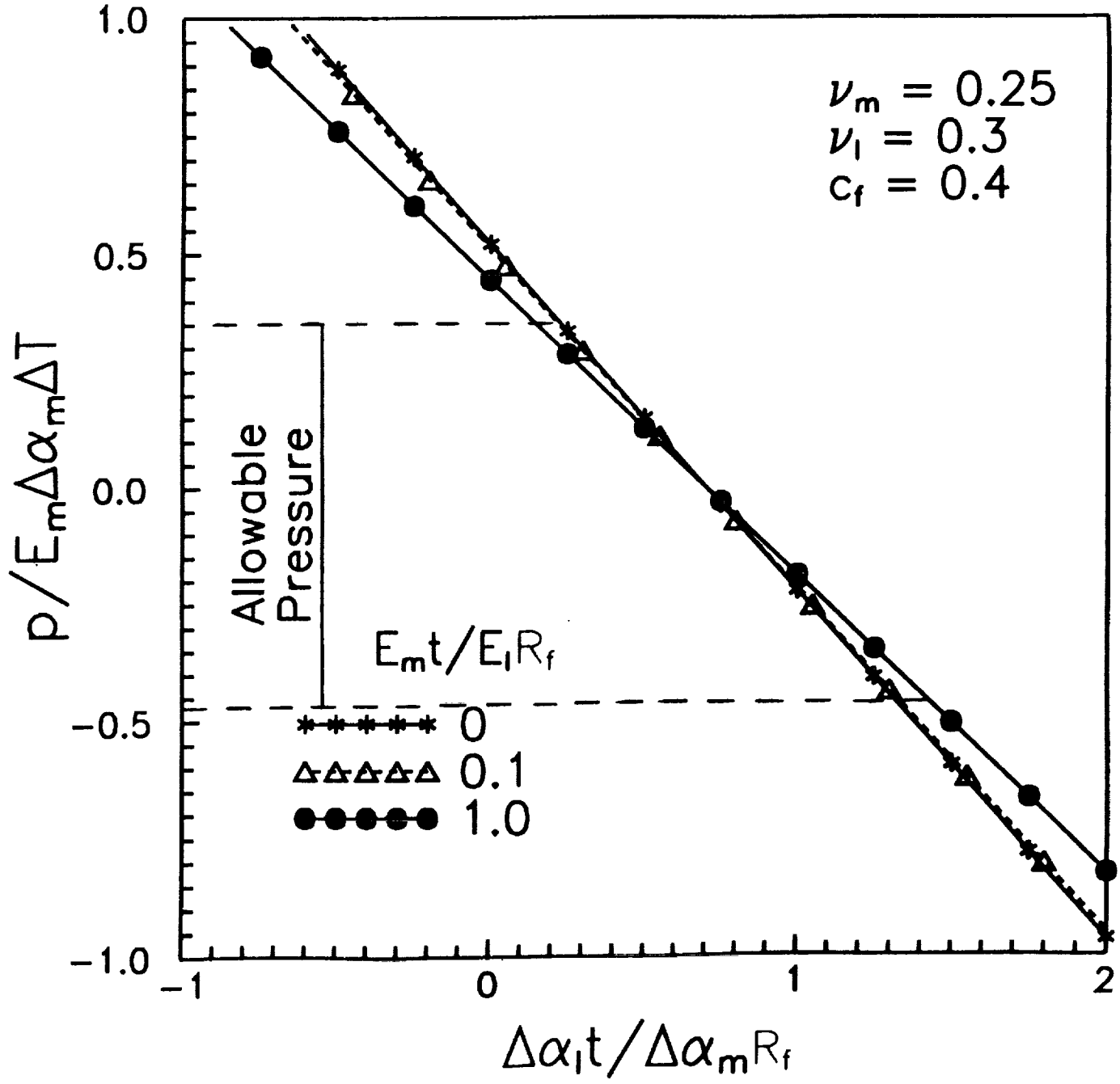

Fig. 3 Normalized pressure as a function of the layer CTE and thickness.

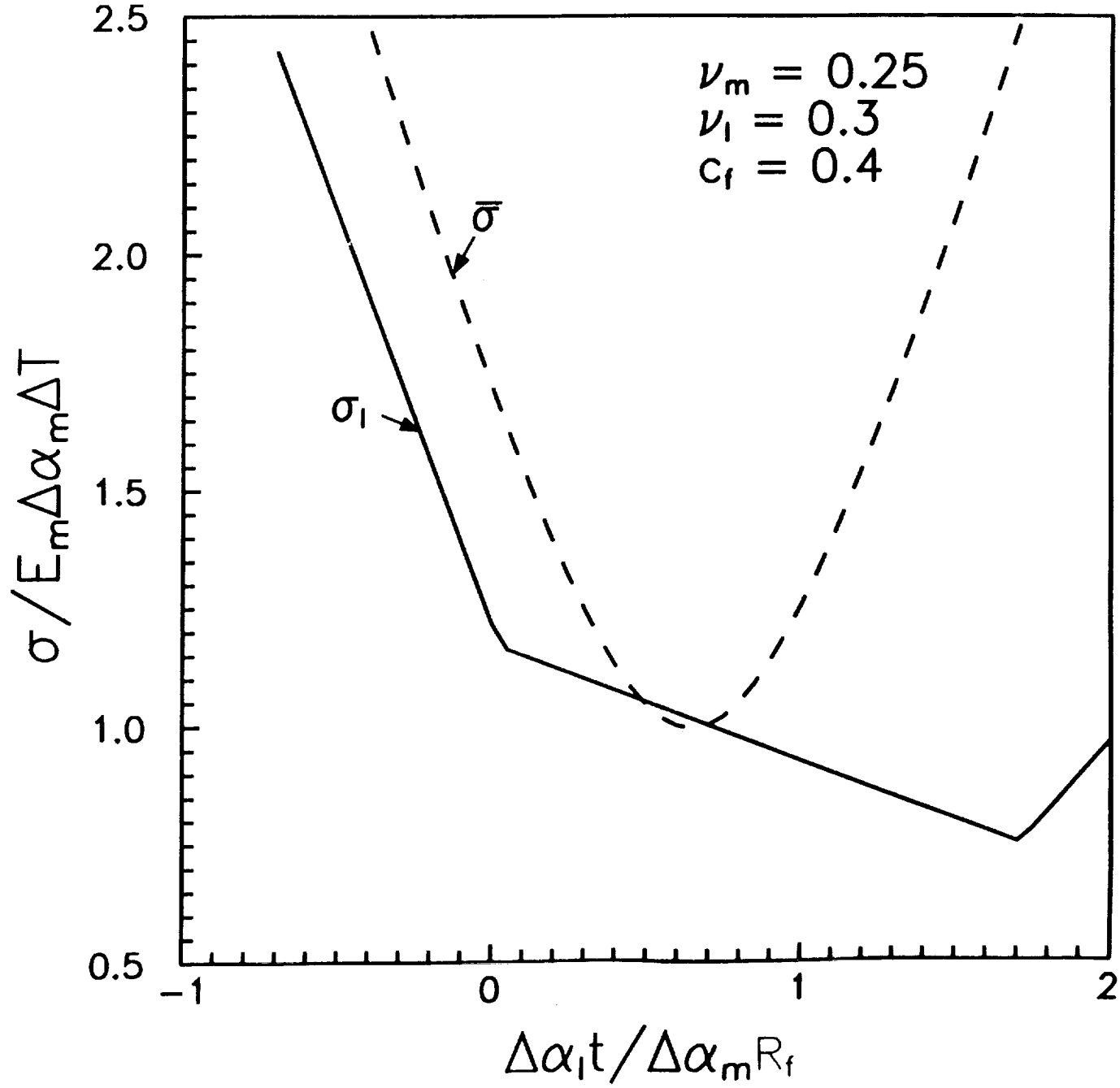

Fig. 4. Maximum principal stress and Mises equivalent stress at the inner surface of the matrix cylinder as a function of the layer CTE and thickness.

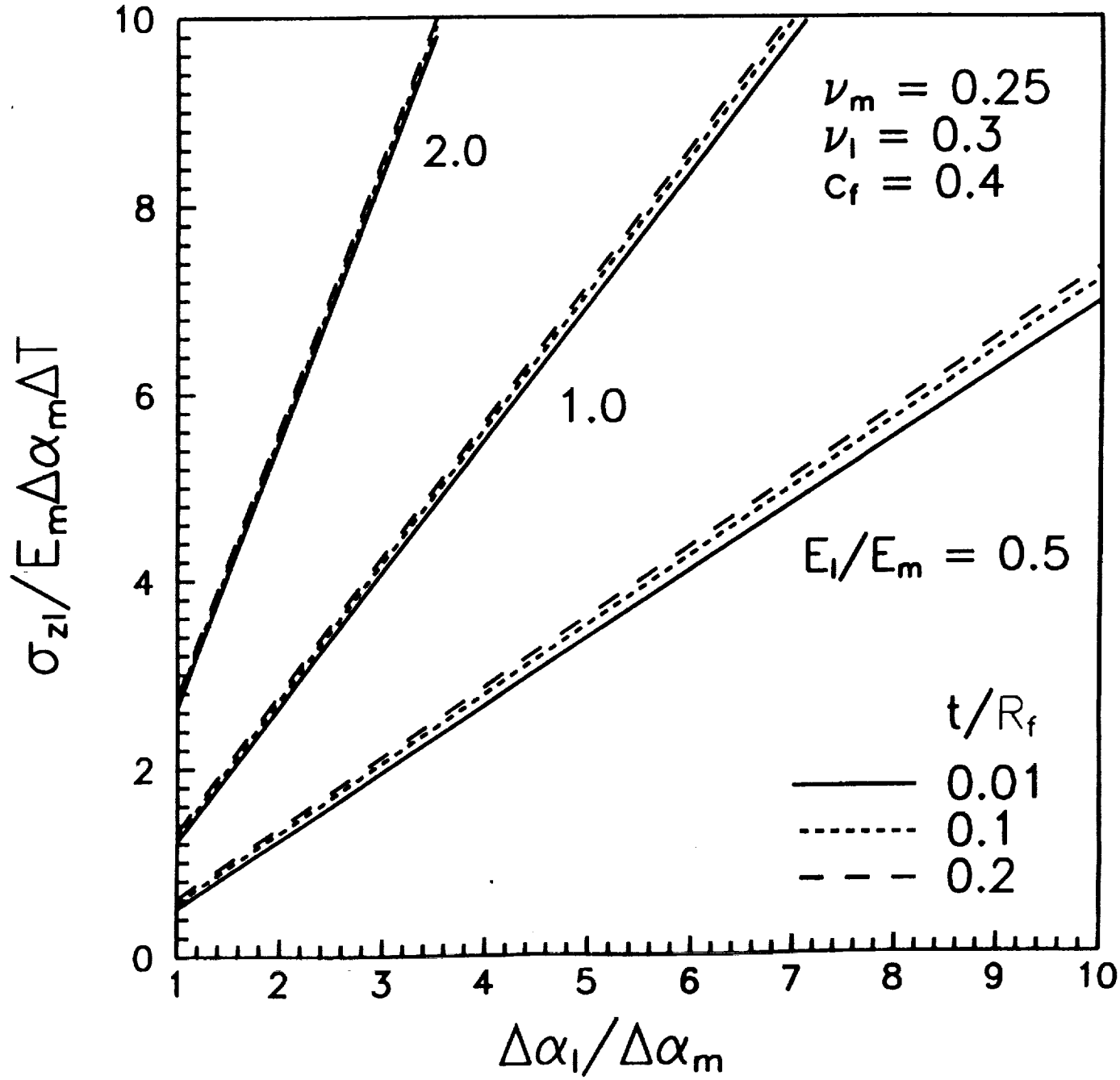

Fig. 5 Longitudinal and hoop tensile stress in interface layer.

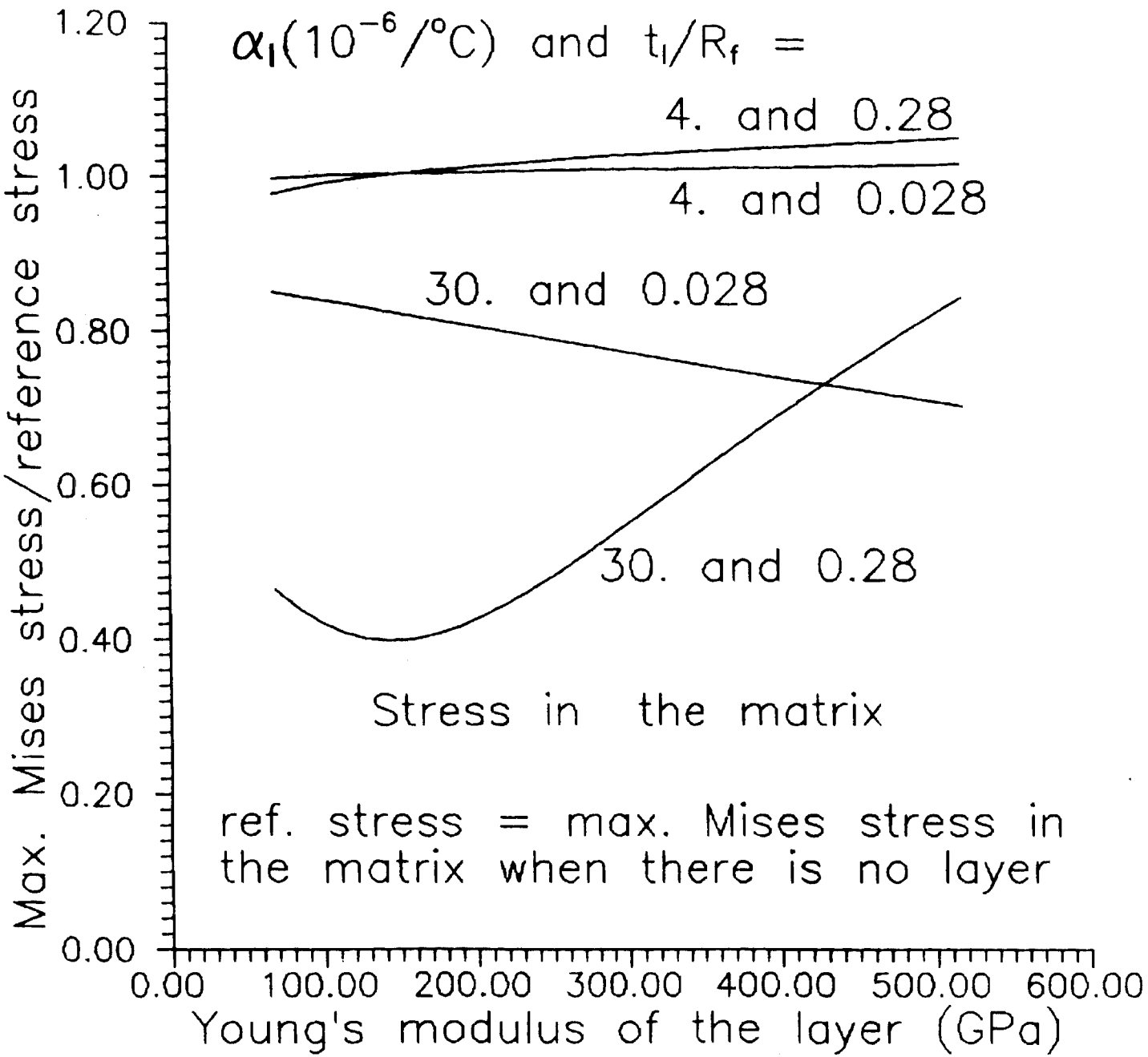

Fig. 6(a) Influence of the layer Young modulus on the stresses in (a) matrix, and (b) layer.

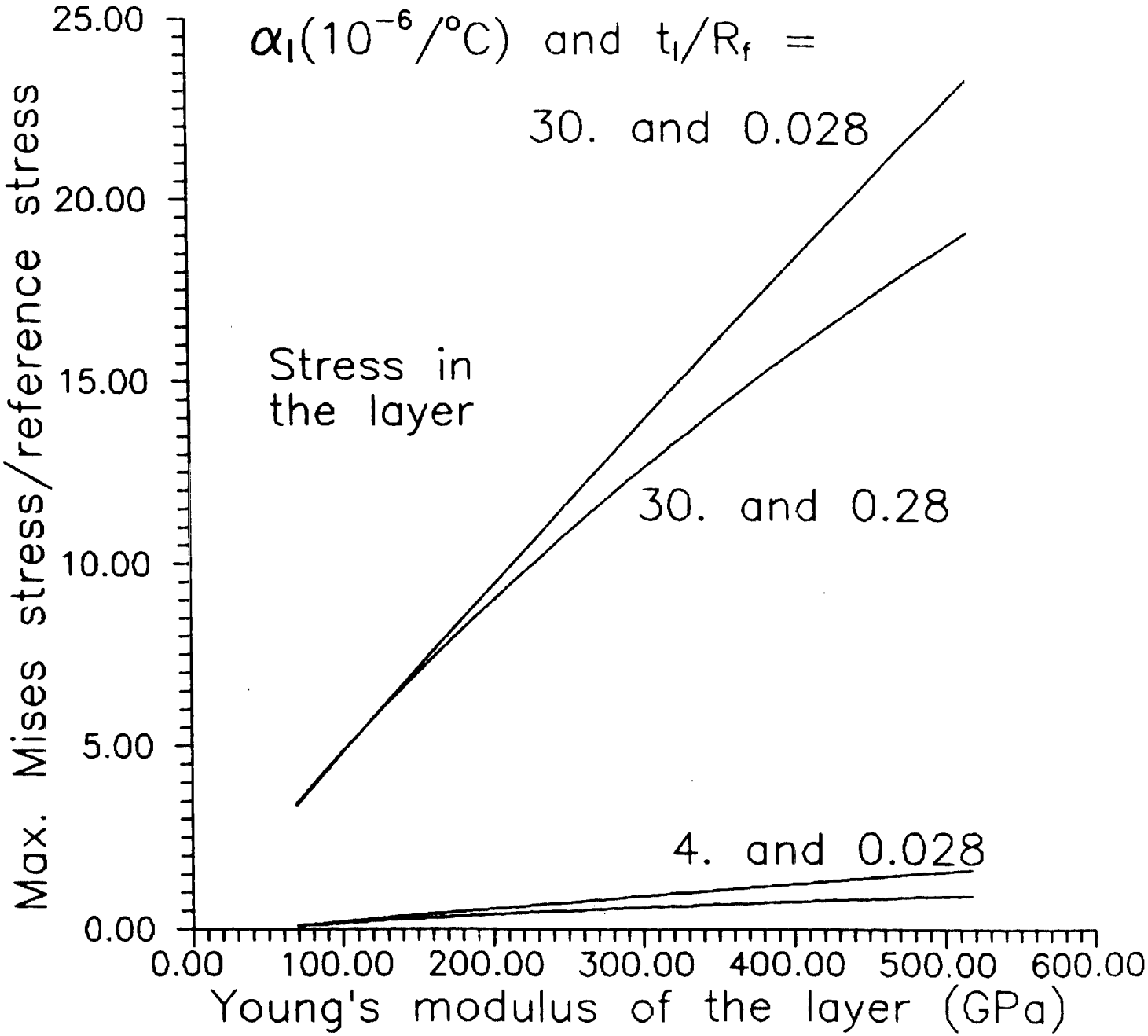

Fig. 6(b) Influence of the layer Young modulus on the stresses in (a) matrix, and (b) layer.

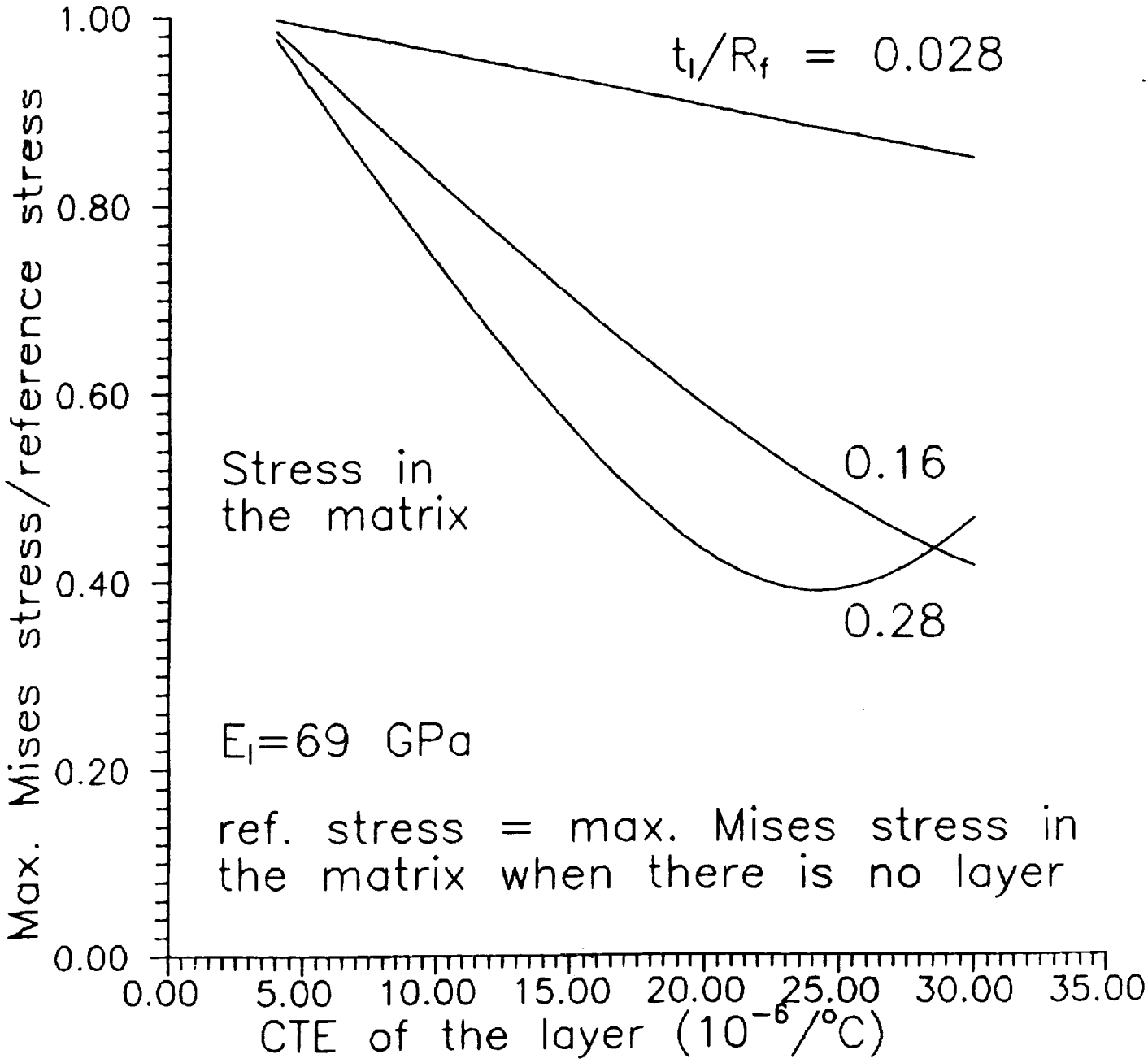

Fig. 7 Influence of the layer CTE on the stresses in the matrix.

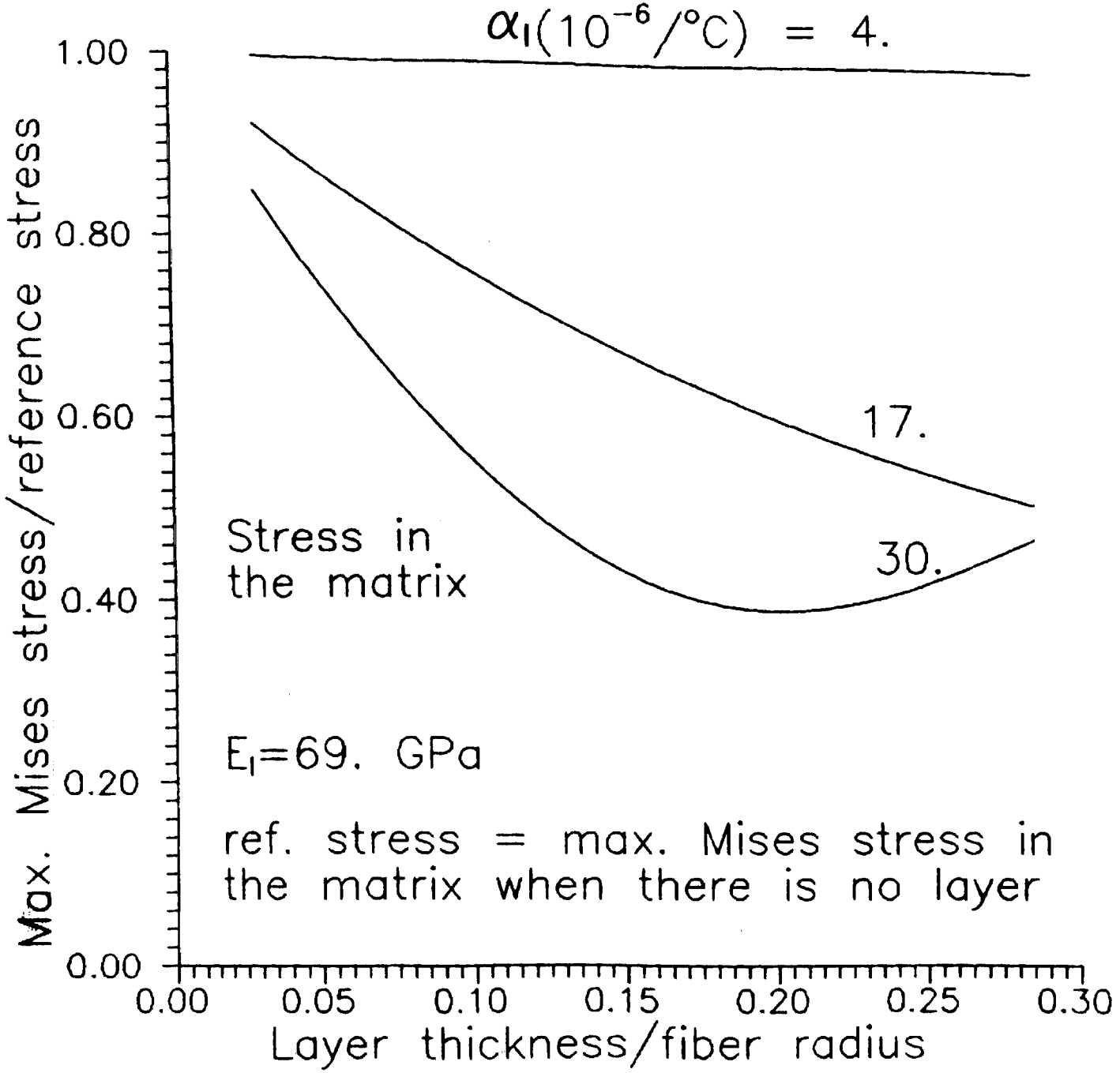

Fig. 8 Influence of the layer thickness on the stresses in the matrix.

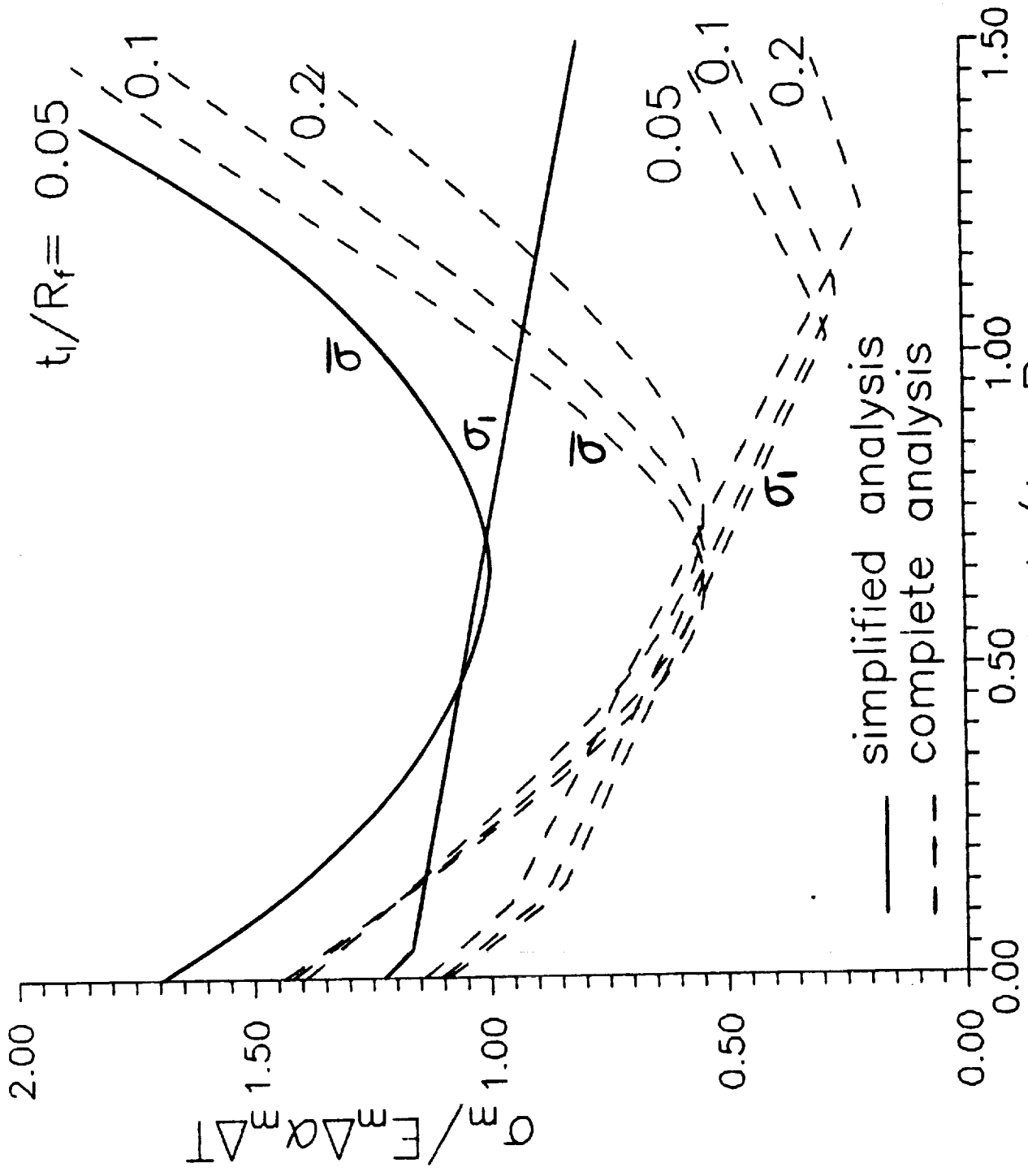

Fig. 9 A convenient parametric representation of the stresses in the matrix.

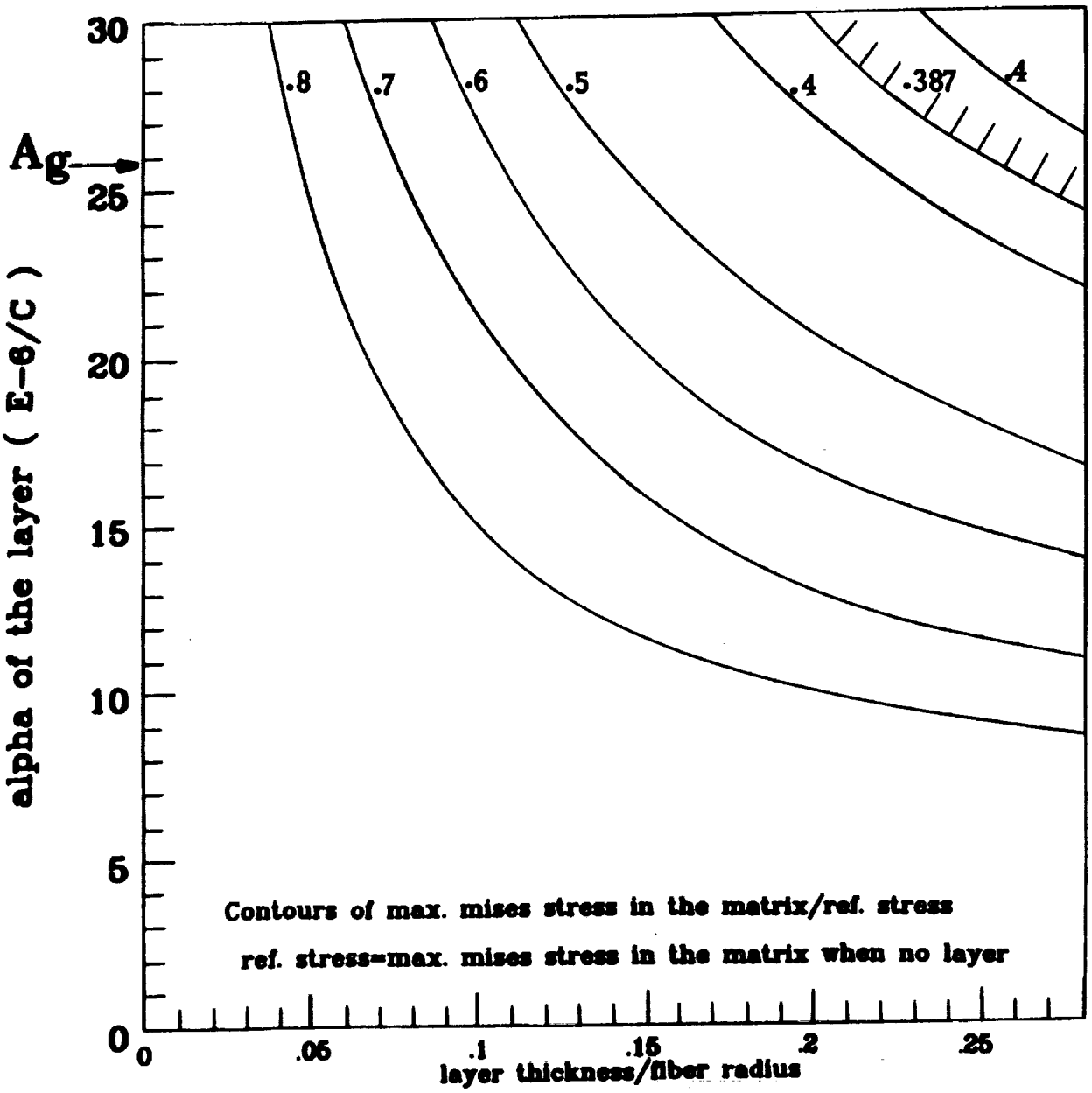

Fig. 10 Contours of constant reduction factor of the Mises equivalent stress in the matrix.

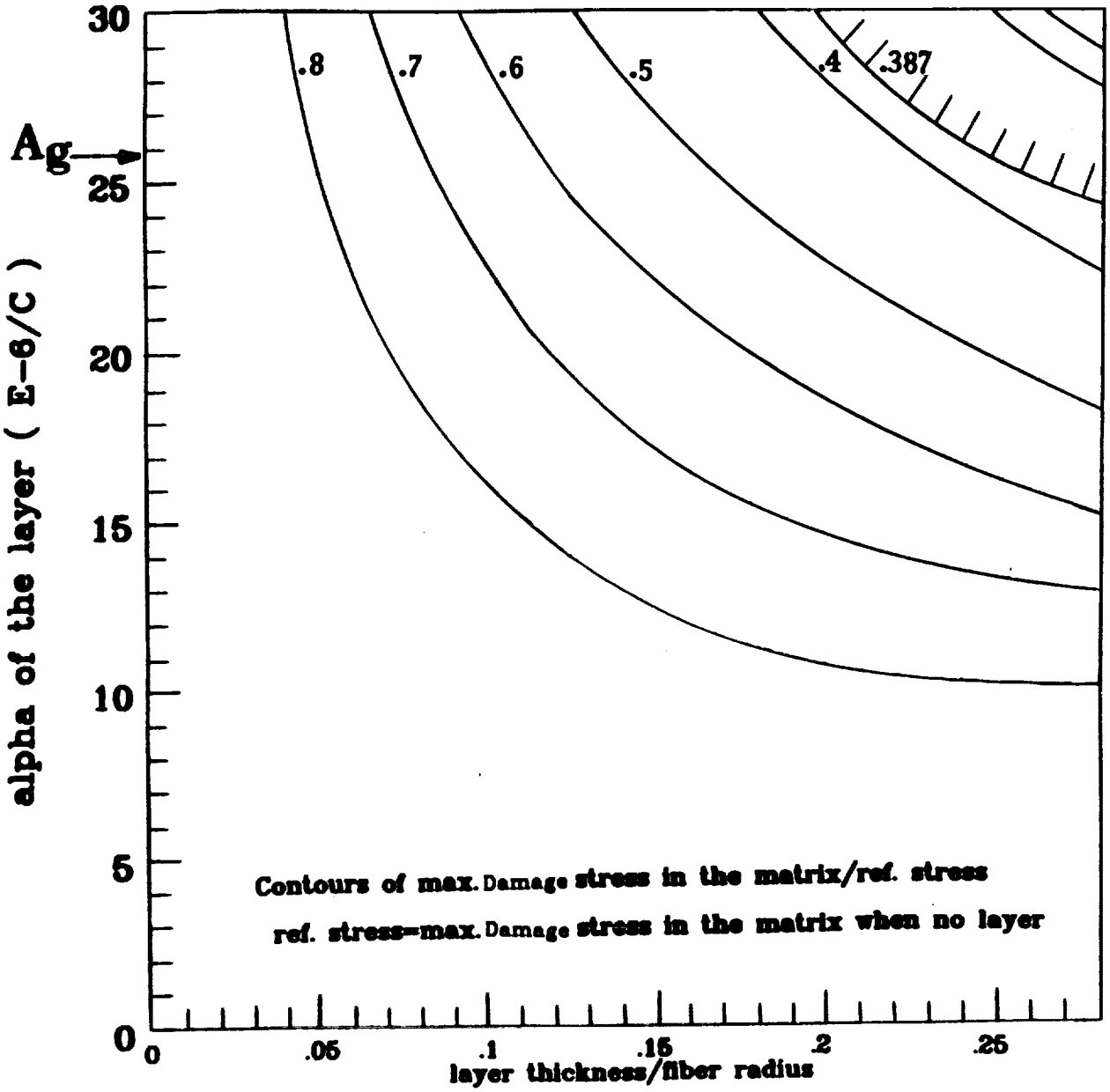

Fig. 11 Contours of constant reduction factor of the damage equivalent stress in the matrix.

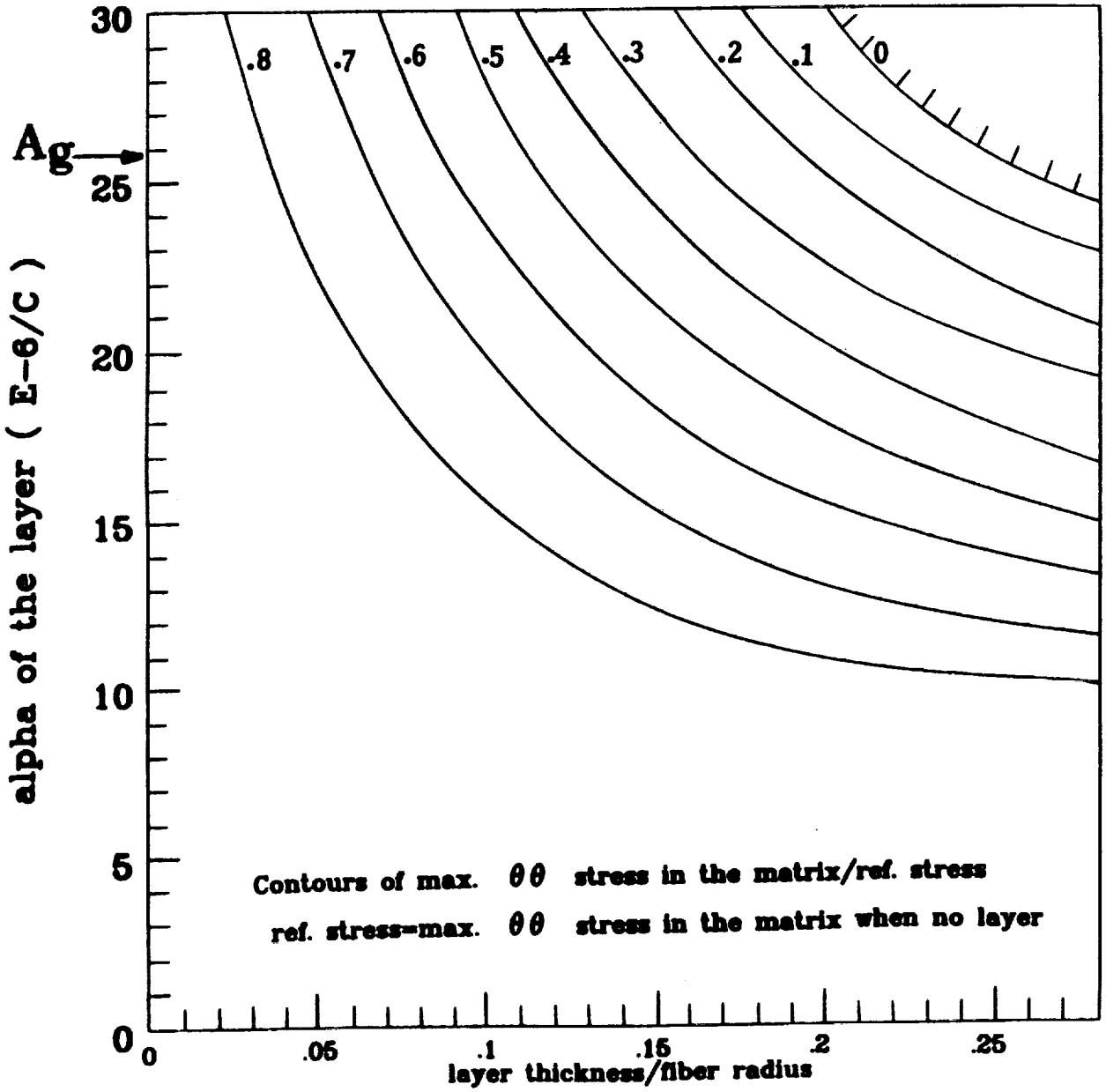

Fig. 12 Contours of constant reduction factor of the hoop stress in the matrix.

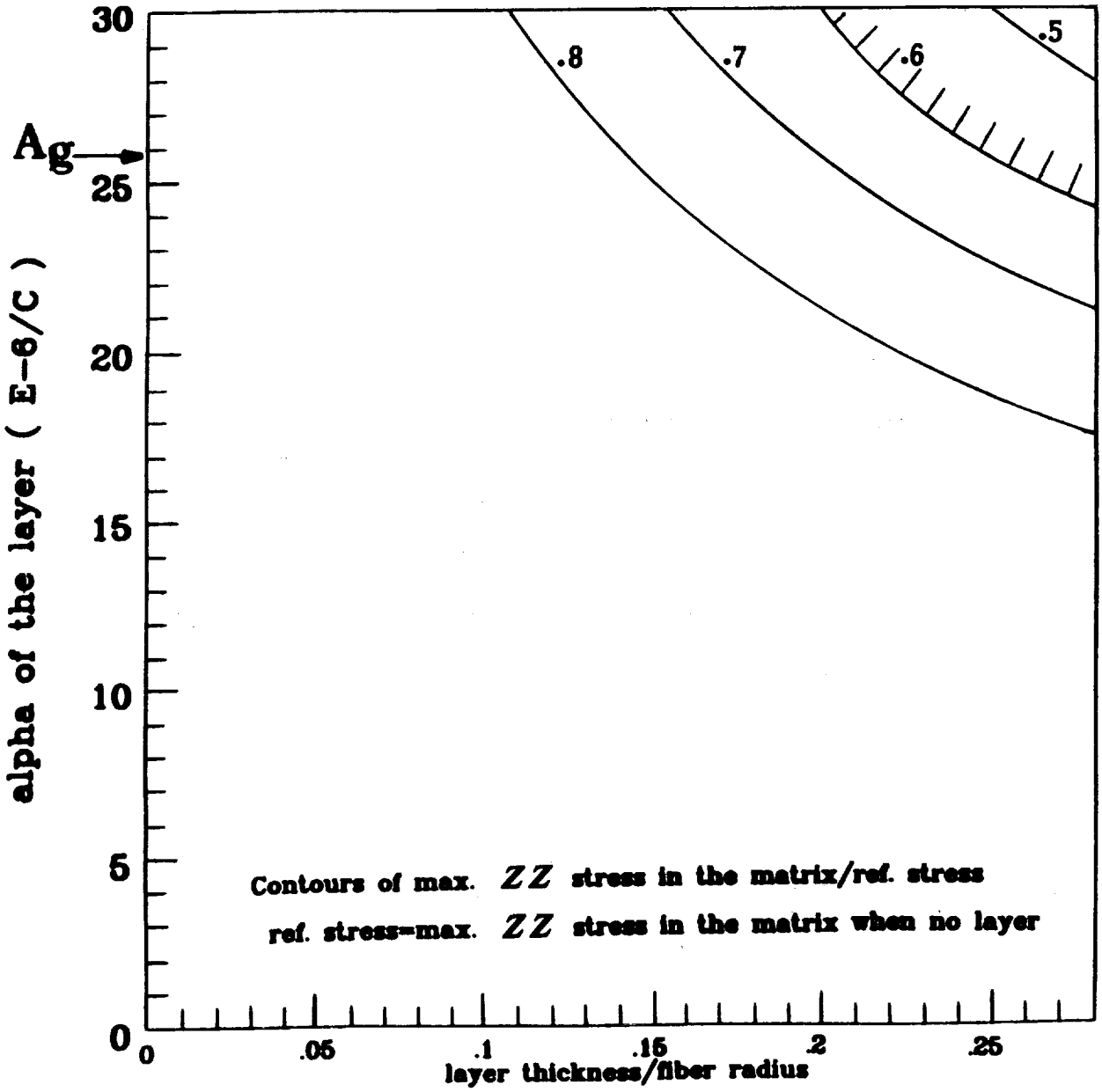

Fig. 13 Contours of constant reduction factor of the axial stress in the matrix.

NASA
National Aeronautics and Space Administration

Report Documentation Page

1. Report No.	2. Government Accession No.	3. Recipient's Catalog No.
NASA CR-185307		

4. Title and Subtitle	5. Report Date
Optimization of Interface Layers in the Design of Ceramic Fiber Reinforced Metal Matrix Composites	November 1990
	6. Performing Organization Code

7. Author(s)	8. Performing Organization Report No.
I. Doghri, S. Jansson, F.A. Leckie, and J. Lemaitre	None
	10. Work Unit No. 510-01-01

9. Performing Organization Name and Address	11. Contract or Grant No.
University of California Department of Mechanical and Environmental Engineering Santa Barbara, California 93106	NAG3-894
	13. Type of Report and Period Covered Contractor Report Final

12. Sponsoring Agency Name and Address	14. Sponsoring Agency Code
National Aeronautics and Space Administration Lewis Research Center Cleveland, Ohio 44135-3191	

15. Supplementary Notes

Project Manager, Steven M. Arnold, Structures Division, NASA Lewis Research Center.

16. Abstract

The potential of using interface layer to reduce thermal stresses in the matrix of composites with a mismatch in coefficients of thermal expansion (CTE) of fiber and matrix has been investigated. It was found that the performance of the layer can be defined by the product of the CTE and the thickness, and that a compensating layer with a sufficiently high CTE can reduce the thermal stresses in the matrix significantly. A practical procedure offering a window of candidate layer materials is proposed.

17. Key Words (Suggested by Author(s))	18. Distribution Statement
Composites; Metallic; Thermal mismatch; Compliant layer; Metal matrix composites	Unclassified – Unlimited Subject Category 24

19. Security Classif. (of this report)	20. Security Classif. (of this page)	21. No. of pages	22. Price*
Unclassified	Unclassified	36	A03

*For sale by the National Technical Information Service, Springfield, Virginia 22161